The Clay Minerals Society Workshop Lectures Series, Vol. 21 (2016), Chapter 8, 87–103

MULTI-SCALE IMAGING AND TRANSPORT PROPERTIES IN SHALES FROM EXPERIMENTS AND MOLECULAR DYNAMICS SIMULATIONS

NATHAN WELCH[1], JOHN CRAWSHAW[1], and EDO BOEK[1,2,*]

[1]*Department of Chemical Engineering, Imperial College London SW7 2AZ, UK*
[2]*Department of Chemistry, University of Cambridge, Lensfield Road, Cambridge CB2 1EW, UK*
[*]*e-mail: esb30@cam.ac.uk*

Transport properties in shales were investigated using experimental and computer-simulation methods. First, an experimental method based on a transient pressure-decay technique was further developed and used instead of classical Darcy core-flood methods. This has allowed measurement of the permeability of tight shale samples on much shorter time scales than by conventional methods. Second, molecular dynamics (MD) computer simulations were used to measure the diffusion coefficients of water and cations in a model clay sample. Measurements of the self-diffusion coefficient showed that the values increased with increasing water content. The results for Na-, Li-, and K-smectites are in satisfactory agreement with experimental and with other simulation results in the literature indicating that the clay interlayer space is an important route of transport for ions and water. The results also lend credibility to the correctness of the diffusion coefficients obtained from the current MD simulations.

1. Introduction

The safe long-term geologic storage of carbon dioxide (CO_2) has become an important scientific issue for implementation of carbon capture and storage (CCS) operations. The formation of an intact and substantial seal above a storage reservoir is required for the initial sealing mechanisms to be effective during CO_2 storage operations (Benson and Cole, 2008). Shales and evaporites are common seal-formation rock types found above numerous storage locations (North, 1985). These seals generally have very low permeabilities. Some also have the tendency to be fissile, however; the formation of micro-fractures within these seals can have a negative effect on the sealing potential of a reservoir and may lead to large areas of high permeability and low capillary pressures compared to the surrounding intact rock (Edlmann *et al*., 2013). The determination of these sealing parameters is important for the selection of suitable sequestration sites. A recent review of available literature for capillary entry-pressure measurements showed a significant shortage of data available for interpretation (Busch and Amann-Hildenbrand, 2013). Numerous experimental techniques have been developed for determining these properties quickly (Hildenbrand *et al.,* 2002; Dong *et al.*, 2005; Egermann *et al*., 2006; Amann et al., 2011; Kohli *et al.*, 2013; Welch *et al*., 2014) with a

DOI: 10.1346/CMS-WLS-21.8

comparative study presented by Boulin *et al*. (2011). Intact-seal samples typically have nm-sized pores as well as very low permeabilities. In order to determine the sealing capacities of shales, their flow properties must be assessed. Although experimental and empirical data are found in the literature, increased fundamental understanding is required. The study of fluid-flow properties and capillary pressure in shales requires specialized equipment and increased complexity in experimental procedure compared to more commonly studied reservoir rocks. The permeability of the systems is often in the nano-Darcy range which makes the measurement of fluid-flow rates, using classic core-flood tests, very difficult. The main difficulty is the large time scale required to obtain accurate measurements. A new, quick experimental method to determine transport properties in shales is described here.

Shales generally contain sand grains accompanied by significant proportions of swelling clays, such as montmorillonite. In the second part of this study an MD simulation is presented, therefore, in which diffusion coefficients are determined because experimental calculation of these values is difficult.

2. Experimental section

The measurement of capillary entry pressure is of great importance to both hydrocarbon-related studies and to carbon sequestration operations. The capillary entry pressure of a sample yields the maximum non-wetting phase pressure that can be maintained within a formation without flow through a reservoir cap rock, often a shale formation. Measurement of this entry pressure is difficult, largely as a result of the sample's low permeability (typically at nano-Darcy level). The low flow rates involved (following Darcy's equation) with shale systems often means that experimental time frames on the order of weeks to months are required.

Experimental techniques have been developed to eliminate the need for extended measurements of low flow rates. The transient pressure-decay method pioneered by Brace *et al*. (1968) has been shown to provide an accurate measurement of extremely low-permeability samples. The technique relies on the extremely low compressibility of water to relate pressure changes within fluid reservoirs connected to the shale sample to the flow rate of fluids through the rock sample. Brace's analysis considers the change in the amount of fluid a rock could contain in a time increment δt, based on changes in both the rock pore space and the fluid's physical properties:

$$\frac{\partial^2 P}{\partial x^2} = \left(\frac{\mu\beta}{k}\right)\left[\frac{\beta_{\text{eff}} - \beta_s}{\beta} + \phi\left(1 - \frac{\beta_s}{\beta}\right)\right]\left(\frac{\partial P}{\partial t}\right) \tag{1}$$

where k is the sample permeability, P is the pressure of the pore fluid, μ is the dynamic viscosity of the fluid, β is the compressibility of the fluid, β_{eff} is the effective compressibility of the rock sample, β_s is the compressibility of the rock material itself, φ is the sample porosity, and δx is an increment in length along the axis of the sample cylinder. Using Laplace transform analysis and a number of assumptions (Brace *et al.,* 1968), this

was shown to yield:

$$(P_{\mathrm{up}} - P_{\mathrm{f}}) = \Delta P\left(\frac{V_{\mathrm{dn}}}{V_{\mathrm{up}} + V_{\mathrm{dn}}}\right)e^{-\alpha t} \tag{2}$$

where V_{up} is the volume of the upstream reservoir, V_{dn} is the volume of the downstream reservoir, P_{f} is the final pressure approached by the system, ΔP is the initial pressure gradient applied across the sample, and

$$\alpha = \left(\frac{kA}{\mu\beta L}\right)\left(\frac{1}{V_1} + \frac{1}{V_2}\right) \tag{3}$$

For detailed analyses of the validity of this solution, readers are referred to studies by Kwon *et al*. (2001) and Welch *et al*. (2016).

An experimental core holder has been developed here which takes advantage of this technique to measure the permeability of several reservoir seal samples and reservoir seal analogues, including a shale sample from the Hontomin CCS project located in Spain. One of the main features of the new apparatus is that the fluid-storage reservoirs are contained within the heated core holder to try and negate temperature effects on the pressure measurement. A simplified diagram of the apparatus is shown in Figure 1 (after Welch *et al*., 2016).

Using this new system, changes in the permeability that occur within shale samples due to varying effective pressures have been measured. For this analysis the simple definition of effective pressure to be the confining pressure applied to the sample plug, minus the pore pressure of the fluid being passed through the shale sample was used. The full permeability–effective pressure relationship can be seen in Figure 2.

The relationship seen in Figure 2 shows the initial decrease in sample permeability as the confining pressure is increased. Then, at a certain point, the trend reverses and an increase in sample permeability is seen. This increase in permeability is thought to be associated with the opening of micro-fractures within the sample which offers an

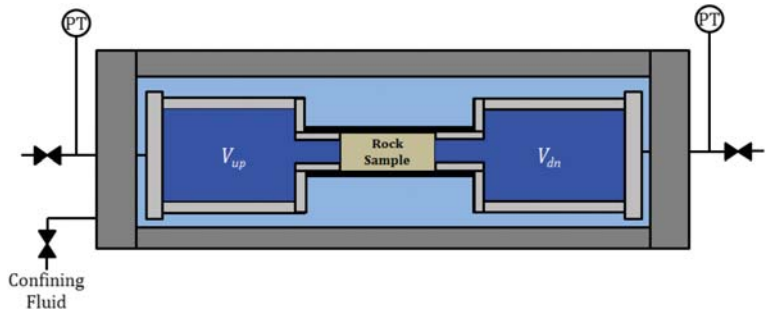

Figure 1. Simplified systemic diagram showing fluid reservoirs used for permeability determination experiments.

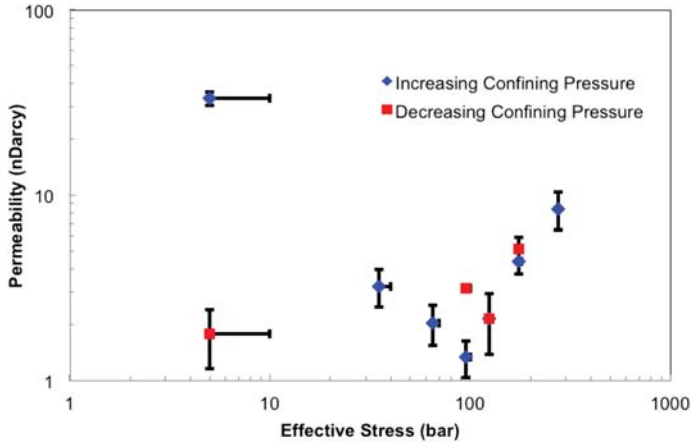

Figure 2. Permeability of the Hontomin shale sample for each effective pressure applied.

increase in transport of fluid through the core. As confining pressure is then decreased again, the permeability of the sample decreases slightly. This decrease is explained as the closure of these micro-fractures as the stress placed on the rock sample is reduced. Then, as confining pressure approaches the initial system stress, the system does not recover to the original permeability. This hysteresis has also been observed in other recent shale experiments (Hol *et al.*, 2012; Liu *et al.*, 2013; Welch *et al.*, 2016). The present authors believe that this is due to the compaction of the sample's grains and narrowing of the pore space. To confirm this hypothesis, direct imaging experiments of the evolution of the micro-fractures as a function of effective stress were required.

X-ray imaging techniques have been developed to investigate the evolution of the structure of shale in the presence of CO_2 (Vega *et al.*, 2014). Using three-dimensional (3D) images of the rock samples, digital rock fluid-flow simulations have been developed to calculate system permeabilities for low-permeability systems, but pore-space imaging remains a substantial hurdle. Micro-computer tomography (CT) techniques used for reservoir-rock characterization lack the capacity to image the pores of many shale samples in the range of <1 μm. Scanning electron microscopy (SEM) has the capability to image features on this length scale, but is limited to 2D surface images. An SEM image of the Hontomin shale sample is shown in Figure 3.

The pore structure is very characteristic of shale samples showing an arrangement of plate-like grains with the pore space being the regions between them. The 3D imaging of nanoporous materials has been advanced significantly with the addition of a focused ion beam (FIB) used for layered milling of samples with sequential SEM imaging to reconstruct the sample pore space (Curtis *et al.*, 2010).

An additional complication involved in dealing with shale systems is the natural reaction that occurs with non-equilibrated fluids, causing either the shrinkage or swelling of

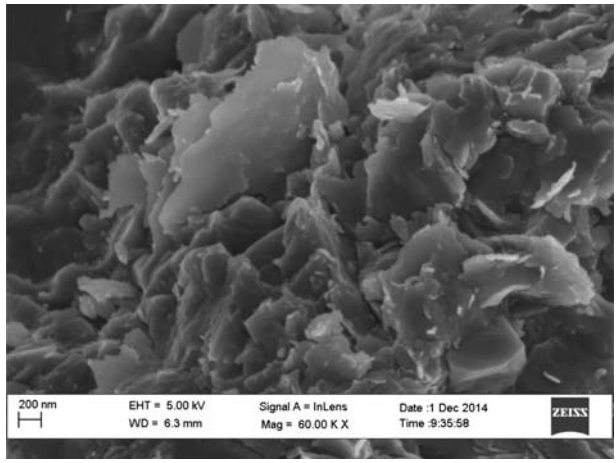

Figure 3. SEM image of the Hontomin shale sample.

clays within the sample. An example of the detrimental effects of these processes can be seen in the tomogram shown in Figure 4. This shale sample was a quarry sample provided from the long lane quarry in the UK, which was fairly consolidated upon arrival. When drilled with tap water, the swelling of the clay occurred within minutes of removal of

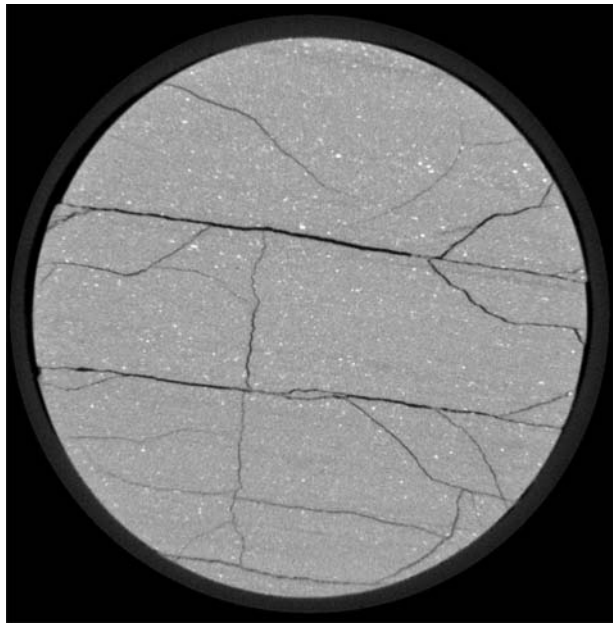

Figure 4. Tomogram of a shale sample after swelling from contact with untreated tap water.

the plug from the coring bit barrel. This caused micro-fracturing of the sample in multiple places both along and perpendicular to the bedding plane of the sample.

A detailed study on micro-fracture evolution with increasing stress, using *in situ* micro-CT imaging, confirming our hypothesis, is in preparation (Welch *et al*., 2016).

Measuring permeability *via* the imaging techniques used is very challenging. In the previous section, significant swelling of the shale sub-samples drilled with tap water was noted, suggesting that a significant fraction of swelling clay exists in the shale sample, affecting shale permeability significantly. This swelling may be due to the uptake of water in the interlamellar space of the clay minerals. Because study of transport processes in the interlamellar space (of the order of nanometers wide) is difficult, MD computer simulations of this process are presented below.

3. Molecular dynamics simulation

The structure of shale is generally described as a matrix of clay layers containing silt particles (Darley and Gray, 1988). Shales containing montmorillonite clays generally have very low permeability. In many cases, clay-mineral content is the major factor affecting shale permeability. As noted in the previous section, the experimental determination of transport properties in shales and clays may be cumbersome. For this reason, MD simulations to calculate transport properties in a model clay sample are described here. The general structure of hydrated montmorillonite is shown in Figure 5 and is discussed further below. No edges exist in this model and the image shows a periodic cell as used in the MD simulations.

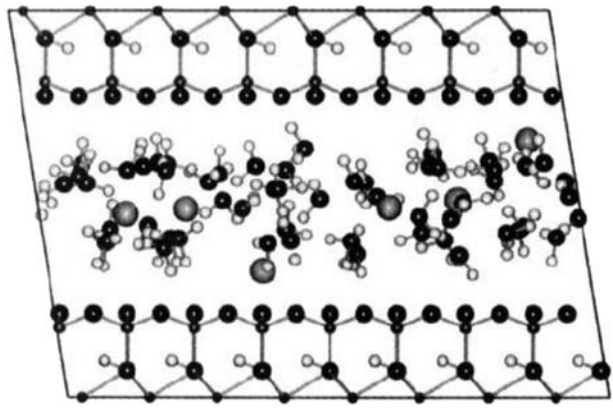

Figure 5. Unit-cell structure of hydrated montmorillonite showing equilibrium configuration of interlayer water molecules and Na^{+} ions (large gray spheres). Oxygen atoms are medium-sized black spheres, H atoms are small white spheres, and both Si and Al ions are small black spheres. Reprinted with the permission of the American Chemical Society from Boek *et al*. (1995).

3.1. Simulation model

The simulation model consists of a clay layer, counterions (Na^+, K^+, or Li^+), and water molecules. The model clay mineral is a Wyoming-type montmorillonite, with unit-cell formula:

$$M_{0.75}[Si_{7.75}Al_{0.25}](Al_{3.5}Mg_{0.5})O_{20}(OH)_4$$

where M represents a monovalent cation: here Na^+, K^+, and Li^+ are considered. This prototypical swelling clay mineral is a member of the smectite family (Newman, 1987) and consists of two tetrahedral sheets, sandwiching an octahedral sheet (2:1). One of eight Al atoms in the octahedral network is substituted randomly by a Mg atom. Likewise, one of 32 Si atoms in the tetrahedral sheet is replaced randomly by an Al atom. These substitutions are typical of a Wyoming-type montmorillonite (Newman, 1987), and give rise to an overall negative charge on the clay framework. This negative charge is balanced by the presence of monovalent interlayer counterions, M. The periodic simulation cell consists of two opposing Wyoming montmorillonite layers measuring 21.12 Å × 18.28 Å, equivalent to eight unit cells. The thickness of one layer is 3.28 Å. Periodic boundary conditions are applied in three dimensions. Thus the model used in the simulations consists of an infinite stack of clay platelets, very similar to a real clay mineral. Note, however, that only basal and interlayer basal surfaces are included, whereas real clay would have edges and external basal surfaces.

The effects of simulation-cell size and shape have been considered and the use of the simulation-cell described above validated by Skipper *et al.* (1995). An equilibrated model of a hydrated K-Wyoming montmorillonite after Monte Carlo (MC) simulation, used as an initial configuration for the current MD simulations, is shown in Figure 5.

3.2. Interaction potential model

The interaction potentials used were the same as in MC simulations reported by Boek *et al.* (1995). The water–water interactions were modeled by the TIP4P model (Jorgensen et *al.*, 1983) which is optimized for bulk water properties. Interactions are pairwise additive and consist of electrostatic and short-range van der Waals attractive and repulsive 6–12 potential terms:

$$v(r) = \sum_{i<j} (q_i q_j / r_{ij} - D_{ij}/r_{ij}^6 + E_{ij}/r_{ij}^{12}) \qquad (4)$$

The water–cation interactions used are compatible with the TIP4P model. For both Na^+ and Li^+ the interactions have the same functional form as in equation 4 (Skipper *et al.*, 1995). For K^+, the potential had a different functional form (Matsouka *et al.*, 1976), including soft exponential repulsions, an attractive r^{-4} term and a repulsive r^{-6} term (see Chandrasekhar *et al.*, 1984, for details). In the MC study (Boek *et al.*, 1995), quantitative agreement was found between experimental and simulated clay layer spacings for water contents increasing from 0 to 100 mg/g clay. This indicates that the TIP4P

parameters used do describe the hydrate structure correctly. This force field should, therefore, be a good basis on which to study the dynamical transport properties in smectite hydrates. The MD simulations of clay hydrates were reported by Chang *et al*. (1995, 1997, 1998) who used the MCY interaction model (Matsouka *et al*., 1976) instead of the TIP4P model (Lie *et al.* 1976). The MCY potential is based on high-quality *ab initio* calculations of the water dimer (Levitt *et al.*, 1997). The thermodynamic properties of bulk liquid water are, however, represented less realistically by MCY than by the TIP4P model; the MCY water model requires a pressure of 850 MPa to maintain a density of 1 g/cm^3 (Matsouka *et al*., 1976), whereas the TIP4P model, used in the current work, requires a pressure of 1 MPa to maintain the liquid density required. On the other hand, the diffusion coefficient for MCY water is in better agreement with the experimental value than that obtained for TIP4P water (Lie *et al*., 1976). The better agreement may be fortuitous and does not, however, justify the use of the MCY potential, for the reasons mentioned above. The TIP4P results are compared below with the MCY model results.

3.3. Molecular dynamics simulations

Over the past two decades, hydrated clay systems have been studied using MD computer simulations (Boek and Sprik, 2003; Churakov, 2006; Suter *et al.*, 2007; Churakov and Gimmi, 2011; Morrow *et al.*, 2013). The *CLAYFF* forcefield is able to predict a range of thermodynamic and structural properties of the interlayer water in clay minerals. Water dynamics in clays have been studied by Marry *et al*. (2006). A thorough investigation of system size, temperature, and water content and their impact on the diffusion of water and cations in clay interlayers was done by Holmboe and Bourg (2014) and the vibrational contribution to the diffusion coefficient from the clay (using the fully flexible *CLAYFF* forcefield) was considerable. The present MD simulations were performed using the parallel computer program, *Moldy*, developed by Refson (1996, 2000), in which molecules are assumed to be rigid bodies, following the classical Newton-Euler equations of motion. As starting models for the MD simulations, equilibrium molecular configurations from Monte Carlo (MC) simulations were used (Boek *et al*., 1995; Watanabe and Klein, 1989). In the MC simulations, the clay interlayer space was allowed to fluctuate. In more detail, the MC simulations were performed in the constant ($N\sigma_{zz}\,T$) ensemble, in which a constant uniaxial stress σ_{zz} of 10^5 Pa was applied perpendicular to the clay layers. Having established the equilibrium interlayer spaces, the current MD simulations were performed in the constant (NVT) ensemble, where the volume V is kept fixed. The temperature of the system was maintained at 298 K by means of coupling to an external heat bath (Nose-Hoover thermostat: Refson, 2000). An integration time step of 0.5 fs was used. Each simulation consisted of an equilibration run of 15 ps, followed by a production run of 400 ps for 32 water molecules (and 800 ps for 64 and 96 water molecules). This corresponds to a water content of $\sim$100 mg/g clay for 32 water molecules (Boek *et al.*, 1995). Note that the clay framework is kept rigid during the simulations. During the production run, configurational data were saved every 100 steps.

3.4. Results: diffusion of water and cations

A quantitative measure of the mobility of cations and water molecules is the self-diffusion coefficient. Self-diffusion coefficients were obtained by monitoring the displacement of a water molecule as a function of time, averaging over all molecules and all choices of time origin, t_0. The mean square displacement (msd) is then calculated as:

$$\langle \Delta r^2(t) \rangle = \langle |r(t_0 + t) - r(t_0)|^2 \rangle \tag{5}$$

Diffusion coefficients, D, were then obtained using the Einstein relation:

$$D = \lim_{t \to \infty} \frac{\langle \Delta r^2(t) \rangle}{6t} \tag{6}$$

As there can be no long-term diffusion perpendicular to the clay layers, the 2D diffusion equation, $\langle \Delta r^2(t) \rangle = 4Dt$, should be used, in fact. In order to permit comparison with experimental results, the 3D Einstein equation (6) is used here, however.

The mean-square displacements of water molecules and cations are displayed as a function of time (Figures 6–8). The slopes of these curves give a quantitative measure of the diffusion coefficients, according to Figure 6, of water and cations for water contents increasing from 32, to 64, to 96 molecules, respectively. Because the statistics of the time correlations deteriorate beyond the half length of the 400 ps runs, only the first 200 ps of correlation time can be used reliably. A least-squares fit to the last 80–90% of the data (up to 200 ps correlation time) yields a best-fit line, which gives a good indication of the long-term diffusive behavior of the water and cations.

The values of the diffusion coefficients obtained for cations DX^+ and water D_W are summarized in Tables 1 and 2, respectively. In general, the values increase with increasing water content, and go toward the bulk water value for the TIP4P model of 3.3×10^{-9} m^2/s (Refson, 2000). The results are compared with experimental values (where available) and with data from other MD simulations using the MCY interaction potential (Chang *et al.,* 1995, 1997, 1998). In general, the current results are in satisfactory agreement with both experiment and simulation. Note that for the Na-monohydrate, the slope of the msd curve shows a kink around a correlation time of 100 ps (see Figure 5). This corresponds with a decrease in the value of D_W from 4.3 to 2.7×10^{-9} m^2/s. Likewise, D_W for the Li-monohydrate shows a decrease from 3.7 to 3.0×10^{-9} m^2/s (Table 2). This change of diffusive regimes may be caused by water diffusing rapidly on short time scales, in local 'cages' of other water molecules, whereas on longer time scales, diffusion is slower because of hindrance by cations and their hydration shells. The transition between these two diffusion regimes occurs at displacements of roughly $\sqrt{30}$ Å for Na^+ and of $\sqrt{25}$ Å for Li^+. This corresponds with local cages of hydrated Na^+ and Li^+ ions of 5.5 Å and 5 Å, respectively. This effect has been observed previously in quasi-elastic neutron scattering (QENS) experiments (Watanabe and Klein, 1989) and MD simulations of hydrated Mg-smectites (Tuck *et al*., 1985). In recent QENS studies of diffusion in clay systems (Curtis *et al.*,

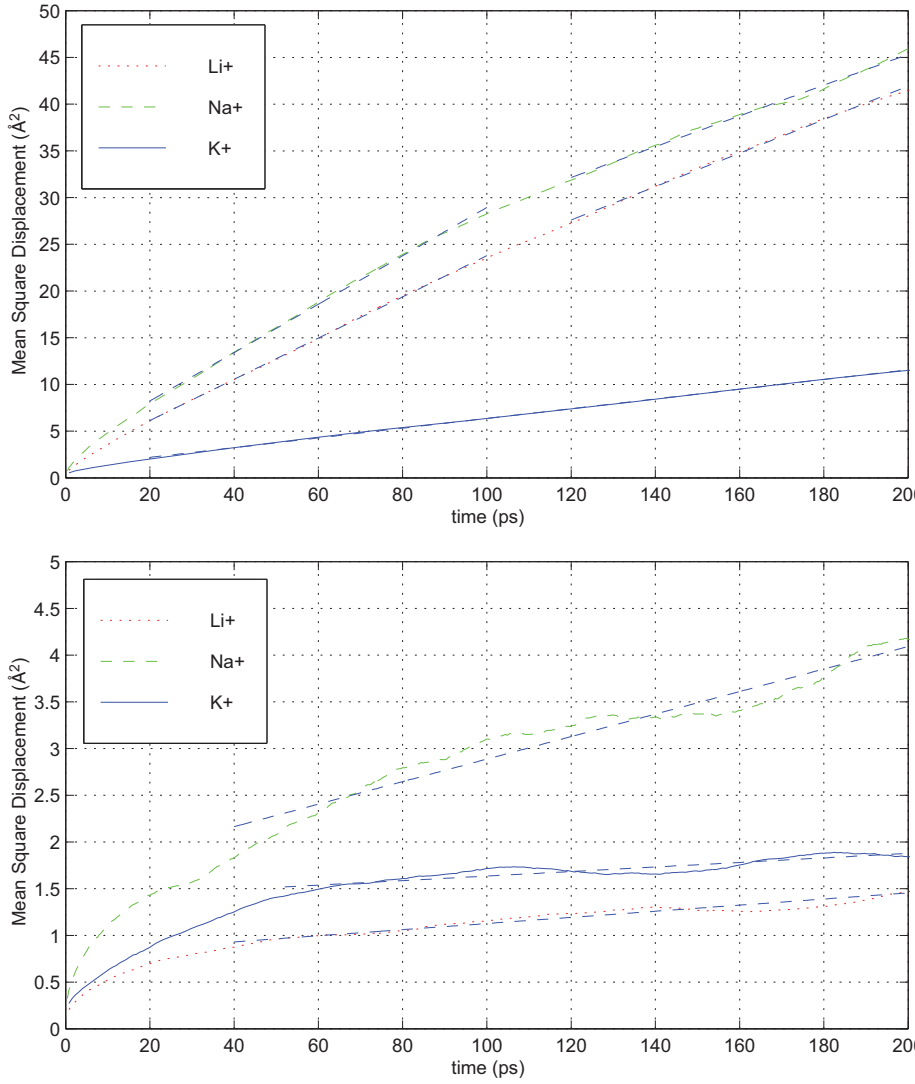

Figure 6. Mean-square displacement of water (upper) and cations (lower) in the interlayer space of Wyoming montmorillonite containing 32 water molecules.

2010), neutron spin echo techniques were used to investigate the anisotropy of diffusion coefficients. The Curtis *et al.* (2010) study also used MD simulations for parameterizing a diffusive model. The K-monohydrate does not show such effects, probably because K^+ ions are weakly hydrated compared to Na^+ and Li^+. An interesting difference also exists between 3 water layers on the one hand, and 1 and 2 layers on the other: the ion-diffusion curves do not saturate in the case of 3 water layers. This implies

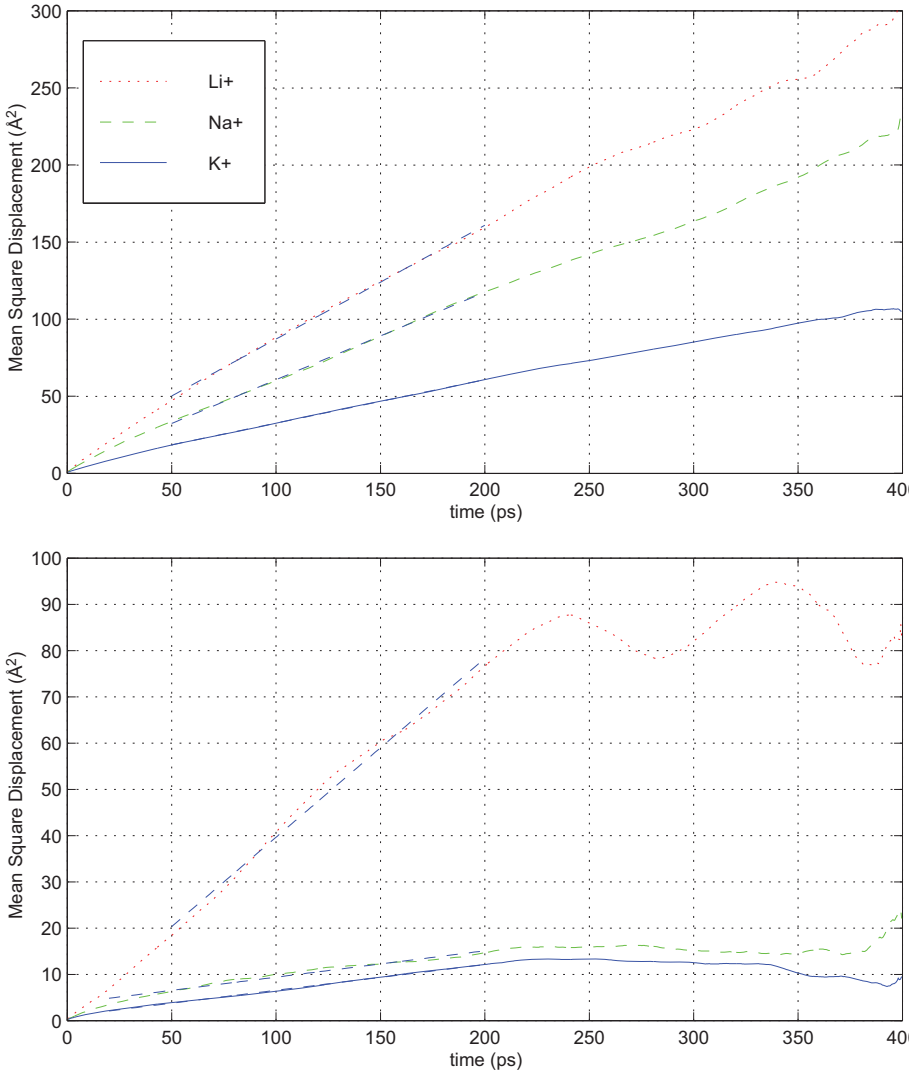

Figure 7. Mean-square displacement of water (upper) and cations (lower) in the interlayer space of Wyoming montmorillonite containing 64 water molecules.

that there is true long-term 3D diffusion for this water content, as the diffusive-layer ions are no longer 'pinned' to the clay surface sites. For the K^+ smectite hydrates, no experimental diffusion data are available, and therefore diffusion coefficients are predicted. The values obtained are in broad agreement with MD simulations using the MCY potential (Chang *et al.*, 1998). The results indicate that water diffusion in the K-smectite hydrates is about half as rapid as in the Li- and Na-smectites.

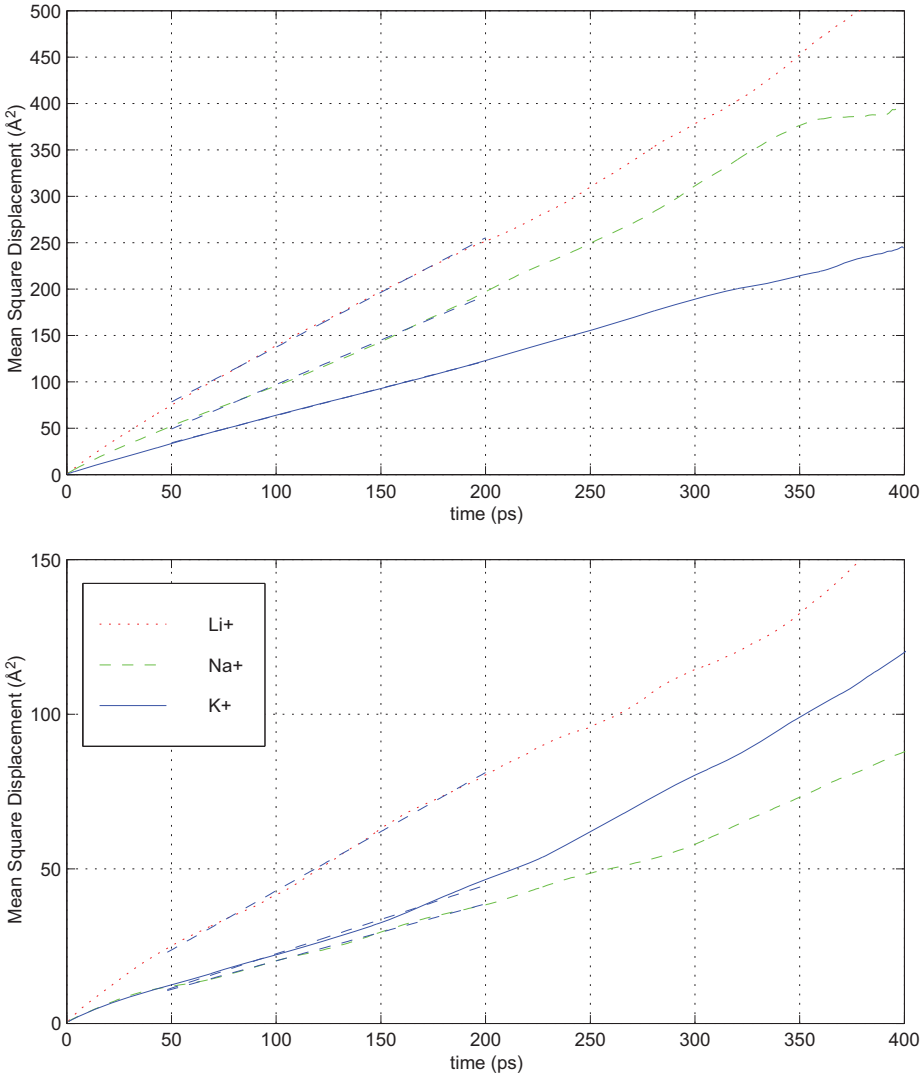

Figure 8. Mean-square displacement of water (upper) and cations (lower) in the interlayer space of Wyoming montmorillonite containing 96 water molecules.

3.5. Comparison with experimental transport coefficients

For comparison with experimental transport coefficients, diffusion through the pore space and the effect of tactoid geometry should be addressed in addition to interlayer-space diffusion. Calculations of diffusivities from sorptivity measurements on compacted clay samples and using soil-physics theory (Denis *et al.*, 1991) indicate that water diffusion increases with increasing K^+/Na^+ counterion fraction. Assuming

Table 1. Self-diffusion coefficients of cations in the interlayer space at 298 K, in units of 10^{-10} m^2/s.

Number of H_2O molecules	D (Li^+) MD	D (Li^+) MD[a]	D (Na^+) MD	D (Na^+) MD[a]	D (Na^+) Expt[b]	D (Na^+) Expt[f]	D (K^+) MD	D (K^+) Expt[c]	D (K^+) MD[d]	D (K^+) Expt[e]
32	0.06	0.11	0.2	0.15	0.1		0.04		1	
64	6.4	0.67	1.0	2.53	1	0.52	0.9		2.5	
96	6.4	4.3	3.1	1.1	2		3.7	1.4	2.4	0.04

[a]MD results from Chang *et al*. (1997); [b]DNa^+(expt) from Nye (1979); [c]DK^+ from Nye (1979); [d]MD results from Chang *et al*. (1998); [e]DK^+ from Sherwood and Craster (2000); [f]DNa^+ from Malikova *et al*. (2006).

that: (1) the clay sample is poorly compacted; and (2) the total volume of a clay sample is roughly independent of counterion chemistry, and using the observation that the volume of the tactoids is larger for Na- than for K-clays (because the interlayer space is larger at the same water content, as observed in the current study), the pore-space fraction in K-clays is concluded to be larger than that in Na-clays. This would explain both the experimentally observed increased water diffusion with increasing K/Na fraction as well as the current simulation results showing slower water diffusion in the interlayer space of K-smectite. The microscopic diffusion coefficients are now compared with experimental values from Sherwood and Craster (2000) on hindered motion of water and ions through a clay membrane. The clay sample is assumed to be well compacted and most water will be present in the interlayer space. The experimental results (Sherwood and Craster, 2000) suggest that the macroscopic diffusion coefficient, obtained from fitting the experimental results to a model of two decaying exponentials and containing three adjustable parameters (the transport coefficients), is of the order of 10^{-12} m^2/s. This is two orders of magnitude smaller than the MD values and the discrepancy may be due to the fact that the experimental clay film, in fact, has a complex tortuous structure and consists of many clay platelets which are aligned, on average, orthogonally to the main direction of mass transport. This conclusion is entirely in agreement with diffusivity measurements on compacted clay samples (Denis *et al*., 1991). In order to make a quantitative comparison between the microscopic (MD) and effective (experimental) diffusion coefficients, D_m and D_e, respectively, a macroscopic model from the literature (Kato *et al*., 1995) is used:

$$D_e = \frac{\varepsilon d}{\tau^2} D_m \tag{7}$$

Table 2. Self-diffusion coefficients of water in the interlayer space at 298 K, in units of 10^{-10} m^2/s.

Number of H_2O molecules	D_W (Li^+) MD	D_W (Li^+) MD[a]	D_W (Li^+) Expt[b]	D_W (Li^+) Expt[c]	D_W (Na^+) MD	D_W (Na^+) MD[a]	D_W (Na^+) Expt[d]	D_W (K^+) MD	D (K^+) MD[e]
32	3.0–3.7	1.3	0.5	4	2.7–4.3	1.0	1–3	0.9	1.3
64	12.3	4.5	2.6	7	9.5	7.9	5–10	4.7	8.5
96	19.7	14		10	16.0	7.2		9.8	9.95

[a]MD results from Chang *et al*. (1997); [b]D_W (expt) from Poinsignon *et al*. (1987); [c]D_W (expt) from Cebula *et al*. (1981); [d]D_W (expt and MD) from Malikova *et al*. (2006); [e]MD results from Chang *et al*. (1998).

where ε is the porosity, d is the constrictivity, and τ is the tortuosity. For isotropic diffusion (Kato *et al*., 1995), τ can be assumed to be $\sim\sqrt{3}$. Using $D_m = 10^{-10}$ m^2/s, $D_e = 10^{-12}$ m^2/s, $\varepsilon = 0.75$, and $\delta = 1$ (as used in Kato *et al*., 1995), a value for the tortuosity of $\tau = 8.7$ was obtained. This value is of the same order of magnitude as found by Kato *et al*. (1995) and suggests that diffusion is anisotropic.

In addition, note that the experimental data (Sherwood and Craster, 2000) have been obtained for flows driven by a gradient in the concentration (or chemical potential, $\Delta\mu$), whereas the current simulations were performed at thermodynamic equilibrium. The connection is provided by Onsager's regression hypothesis: the relaxation of macroscopic non-equilibrium disturbances is governed by the same laws as the regression of spontaneous microscopic fluctuations in an equilibrium system (Chandler, 1987). This hypothesis, which is an important consequence of the fluctuation-dissipation theorem, is rigorous in the linear (low gradient) regime. As a recommendation for future work, calculation of gradient-driven diffusion using MD simulations and Onsager's regression hypothesis would be useful.

4. Conclusions

Experimental investigations were carried out to determine the permeability of real shale samples using a novel transient method instead of classical core-flood experiments. Significant swelling of the shale sub-samples drilled with tap water was observed,

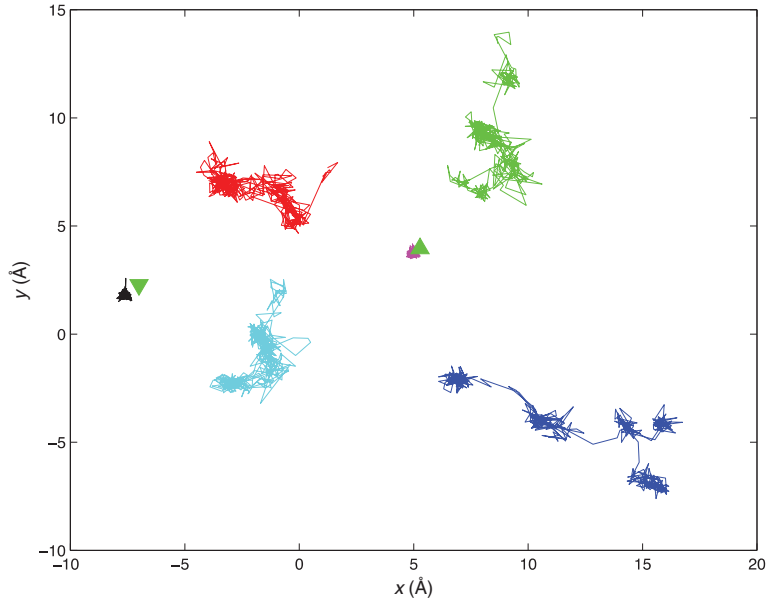

Figure 9. MD trajectories for Na^+ counterions in the single-layer hydrate.

suggesting that there is a significant fraction of swelling clay in the shale sample which affects shale permeability. This swelling may be due to the uptake of water in the interlamellar space of the clay minerals. Transport processes in the interlamellar space (nm wide) using experimental methods are difficult to study. Molecular dynamics computer simulations of this process were used, therefore, to determine the transport properties of cations and water molecules in hydrated Li-, Na-, and K-smectite clays. Measurements of the self-diffusion coefficient show that the values increase with increasing water content. The results for Na-, Li-, and K-smectites are in satisfactory agreement with experiment and other simulation results in the literature, indicating that the clay interlayer space is an important route of transport for ions and water, and lends credibility to the correctness of the diffusion coefficients obtained from the current simulations. Diffusion coefficients for K-smectite hydrates are predicted which have yet to be verified experimentally.

Note that the size of the simulation box and simulation timescale used here may not be sufficient to capture the macroscopic diffusion behavior completely. Note that the jump diffusion behavior is captured in Figure 9, even on time scales of <0.5 ns.

Comparison with clay-film diffusion experiments suggests that the experimental diffusion is anisotropic and the value of the tortuosity obtained may be used to estimate shale permeability in future work.

Acknowledgments

Guest editor: H.C. Greenwell

The authors and editors are grateful to anonymous reviewers who offered very helpful input and suggestions. A list of all reviewers is given at the end of the Preface for this volume.

References

Amann, A., Waschbüsch, M., Bertier, P., Busch, A., Krooss, B.M., and Littke, R. (2011) Sealing rock characteristics under the influence of CO_2. *Energy Procedia*, **4**, 5170–5177.

Benson, S.M. and Cole, D.R. (2008) CO_2 sequestration in deep sedimentary formations. *Elements*, **4**, 325–331.

Boek, E.S. and Sprik. M. (2003) *Ab initio* molecular dynamics study of the hydration of a sodium smectite clay. *The Journal of Physical Chemistry B*, **107**, 3251–3256.

Boek, E.S., Coveney, P.V., and Skipper, N.T. (1995) Monte Carlo molecular modeling studies of hydrated Li-, Na-, and K-smectites: Understanding the role of potassium as a clay swelling inhibitor. *Journal of the American Chemical Society*, **117**, 12608–12617.

Boulin, P., Bretonnier, P., Vassil, V., Samouillet, A., Fleury, M., and Lombard, J. (2011) Entry pressure measurements using three unconventional experimental methods. Presented at the International Symposium of the Society of Core Analysts, Austin, Texas, USA.

Bounds, D.G. (1985) A molecular dynamics study of the structure of water around the ions Li^+, Na^+, K^+, Ca^{++}, Ni^{++} and Cl^-. *Molecular Physics,* **54**, 1335–1355.

Brace, W.F., Walsh, J.B., and Frangos, W.T. (1968) Permeability of granite under high pressure. *Journal of Geophysical Research*, **73**, 2225–2236.

Busch, A. and Amann-Hildenbrand, A. (2013) Predicting capillarity of mudrocks. *Marine and Petroleum Geology*, **45**, 208–223.

Cebula, D.J., Thomas, R.K., and White, J.W. (1981) Diffusion of water in Li montmorillonite studied by quasi-elastic neutron scattering. *Clays and Clay Minerals*, **29**, 241–248.

Chandler, D. (1987) *Introduction to Modern Statistical Mechanics*. Oxford University Press, Oxford, UK.

Chandrasekhar, J., Spellmeyer, D.C., and Jorgensen, W.L. (1984) Energy component analysis for dilute aqueous solutions of Li^+, Na^+, F^-, and Cl^- ions. *Journal of the American Chemical Society*, **106**, 903–910.

Chang, F.-R.C., Skipper, N.T., and Sposito, G. (1995) Computer simulation of interlayer molecular structure in sodium montmorillonite hydrates. *Langmuir,* **11**, 2734–2741.

Chang, F.-R.C., Skipper, N.T., and Sposito, G. (1997) Monte Carlo and molecular dynamics simulations of interfacial structure in lithium-montmorillonite hydrates. *Langmuir*, **13**, 2074–2082.

Chang, F.-R.C., Skipper, N.T., and Sposito, G. (1998) Monte Carlo and molecular dynamics simulations of electrical double-layer structure in potassium-montmorillonite hydrates. *Langmuir*, **14**, 1201–1207.

Churakov, S.V. (2006) Ab initio study of sorption on pyrophyllite: Structure and acidity of edge sites. *The Journal of Physical Chemistry B*, **110**, 4135–4146.

Churakov, S.V. and Gimmi, T. (2011) Up-scaling of molecular diffusion coefficients in clays: A two-step approach. *The Journal of Physical Chemistry C*, **115**, 6703–6714.

Curtis, M.E., Ambrose, R.J., and Sondergeld, C.H. (2010) Structural characterization of gas shales on the micro-and nano-scales. Canadian Unconventional Resources and International Petroleum Conference, Society of Petroleum Engineers.

Darley, H.C. and Gray, G.R. (1988) *Composition and Properties of Drilling and Completion Fluids*. Gulf Professional Publishing, Houston, Texas, USA.

Denis, J.H., Keall, M.J., Hall, P.L., and Meeten, G.H. (1991) *Clay Minerals,* **26**, 255–268.

Edlmann, K., Haszeldine, S., and McDermott, C. (2013) Experimental investigation into the sealing capability of naturally fractured shale caprocks to supercritical carbon dioxide flow. *Environmental Earth Sciences*, **70**, 3393–3409.

Egermann, P., Lombard, J., and Bretonnier, P. (2006) A fast and accurate method to measure threshold capillary pressure of caprocks under representative conditions. SCA2006–07, Society of Core Analysts.

Greathouse, J.A., Refson, K., and Sposito, G. (2001) Molecular dynamics simulation of water mobility in magnesium-smectite hydrates. *Journal of the American Chemical Society,* **122**, 11459–11464.

Hall, P.L., Ross, D.K., Tuck, J.J., and Hayes, M.H.B. (1978) Dynamics of interlamellar water in divalent cation exchanged expanding lattice clays. Pp. 617–635 in: *Proceedings of the IAEA Symposium* 'Neutron Inelastic Scattering', Vienna, 1977. International Atomic Energy Agency, Vienna, Vol. **1**.

Hildenbrand, A., Schlömer, S., and Krooss, B. (2002) Gas breakthrough experiments on fine-grained sedimentary rocks. *Geofluids*, **2**, 3–23.

Hol, S., Peach, C., and Spiers, C.J. (2012) Direct coupling between stress, strain and adsorption reactions – A study on coal-CO_2 systems. AGU Fall Meeting Abstracts, **1**, p. 2470.

Holmboe, M. and Bourg, I. (2014) Molecular dynamics simulations of water and sodium diffusion in smectite interlayer nanopores as a function of pore size and temperature. *The Journal of Physical Chemistry C*, **118**, 1001–1013.

Jorgensen, W.L., Chandrasekhar, J., Madura, J.D., Impey, R.W., and Klein, M.L.J. (1983) Comparison of simple potential functions for simulating liquid water. *The Journal of Chemical Physics,* **79**, 926–935.

Kato, H., Muroi, M., Yamada, N., Ishida, H., and Sato, H. (1995) Estimation of effective diffusivity in compacted bentonite. Pp. 277–284 in: *Scientific Basis for Nuclear Waste Management*, vol. **18** (T. Murakami and R.C. Ewing, editors). Materials Research Society, Pittsburgh, Pennsylvania, USA.

Kohli, A.H. and Zoback, M.D. (2013) Frictional properties of shale reservoir rocks. *Journal of Geophysical Research: Solid Earth*, **118**, 5109–5125.

Kwon, O., Kronenberg, A.K., Gangi, A.F., and Johnson, B. (2001) Permeability of Wilcox shale and its effective pressure law. *Journal of Geophysical Research*, **106**, 19339–19353.

Levitt, M., Hirshberg, M., Sharon, R., Laidig, K., and Daggett, V. (1997) Calibration and testing of a water model for simulation of the molecular dynamics of proteins and nucleic acids in solution. *The Journal of Physical Chemistry B,* **101**, 5051–5061.

Li, S., Dong, M., Li, Z., Huang, S., Qing, H., and Nickel, E. (2005) Gas breakthrough pressure for hydrocarbon reservoir seal rocks: implications for the security of long-term CO_2 storage in the Weyburn field. *Geofluids*, **5**, 326–334.

Lie, G.C., Clementi, E., and Yoshimine, M. (1976) Study of the structure of molecular complexes. XIII. Monte Carlo simulation of liquid water with a configuration interaction pair potential. *The Journal of Chemical Physics,* **64**, 2314–2323.

Liu, F., Ellett, K., Xiao, Y., and Rupp, J.A. (2013) Assessing the feasibility of CO_2 storage in the New Albany Shale (Devonian–Mississippian) with potential enhanced gas recovery using reservoir simulation. *International Journal of Greenhouse Gas Control*, **17**, 111–126.

Malikova, N., Cadène, A. Marry, V., Dubois, E., and Turq, P. (2006) Diffusion of water in clays on the microscopic scale: Modeling and experiment. *The Journal of Physical Chemistry B,* **110**, 3206–3214.

Marry, V., Dubois, E., Malikova, N., Breu, J., and Haussler, W. (2013) Anisotropy of water dynamics in clays: Insights from molecular simulations for experimental QENS analysis. *Journal of Physical Chemistry C*, **117**, 15106–15115.

Matsouka, O., Clementi, E., and Yoshimine, M. (1976) Cl study of the water dimer potential surface. *The Journal of Chemical Physics,* **64**, 1351–1361.

Morrow, C.P., Yazaydin, A.O., Krishnan, M., Bowers, G.M., Kalinichev, A.G., and Kirkpatrick, R.J. (2013) Structure, energetics, and dynamics of smectite clay interlayer hydration: Molecular dynamics and metadynamics investigation of Na-hectorite. *The Journal of Physical Chemistry C*, **117**, 5172–5187.

Newman, A.C.D. (1987) *Chemistry of Clays*. Monograph **6**, Mineralogical Society, London.

North, F.K. (1985) *Petroleum Geology*, 2nd edition. Allen & Unwin, Winchester, Massachusetts, USA.

Nye, P.H. (1979) Diffusion of ions and uncharged solutes in soils and soil clays. *Advances in Agronomy,* **31**, 225–272.

Poinsignon, C., Estrade-Szwarckopf, J., Conard, J., and Dianoux, A.J. (1987) Water dynamics in the clay water system: A quasi-elastic neutron scattering study. Pp. 284–291 in: *Proceedings of the International Clay Conference*, Denver (L.G. Schultz, H. van Olphen, and F.A. Mumpton, editors). The Clay Mineral Society, Bloomington, Indiana, USA.

Refson, K. (1996) *Moldy User's Manual.* Release Revision: 2.12; Department of Earth Sciences, Parks Road, Oxford, UK.

Refson, K. (2000) Moldy: a portable molecular dynamics simulation program for serial and parallel computers. *Computer Physics Communications*, **126**, 310–329.

Sherwood, J. and Craster, B. (2000) Transport of water and ions through a clay membrane. *Journal of Colloid and Interface Science,* **230**, 349–358.

Skipper, N.T., Chang, F.-R.C., and Sposito, G. (1995) Monte Carlo simulation of interlayer molecular structure in swelling clay minerals. 1. Methodology. *Clays and Clay Minerals,* **43**, 285–293.

Suter, J.L., Coveney, P.V., Greenwell, H.C., and Thyveetil, M.A. (2007) Large-scale molecular dynamics study of montmorillonite clay: Emergence of undulatory fluctuations and determination of material properties. *The Journal of Physical Chemistry C*, **111**, 8248–8259.

Tuck, J.J., Hall, P.L., Hayes, M.H.B., Ross, D.K., and Hayter, J.B. (1985) Quasi-elastic neutron-scattering studies of intercalated molecules in charge-deficient layer silicates. 2. High-resolution measurements of the diffusion of water in montmorillonit and vermiculite. *Journal of the Chemical Society, Faraday Transactions I*, **81**, 833–846.

Vega, B., Dutta, A., and Kovscek, A.R. (2014) CT imaging of low-permeability, dual-porosity systems using high X-ray contrast gas. *Transport in Porous Media*, **101**, 81–97.

Watanabe, K. and Klein, M.L. (1989) Effective pair potentials and the properties of water. *Chemical Physics,* **131**, 157–167.

Welch, N.J., Crawshaw, J.P., and Boek, E.S. (2014) Comparison of the change of cap rock permeability and capillary entry pressure with varying effective stress. SCA2014-085, Society of Core Analysts.

Welch, N., Crawshaw, J.P., and Boek, E.S. (2016) in press.